

# Distinct Element Modelling of a Landslide Triggered by the 5.12 Wenchuan Earthquake: A Case Study

Zhi-Chen Song · Lian-Heng Zhao · Liang Li · Yingbin Zhang · Gaopeng Tang

Received: 12 August 2017 / Accepted: 19 January 2018 / Published online: 24 February 2018  
© Springer International Publishing AG, part of Springer Nature 2018

**Abstract** The Donghekou landslide, which was triggered by the 2008 Wenchuan earthquake, was estimated to have a volume of 24 million cubic meters and resulted in numerous properties and lives lost. The landslide is considered a typical rapid long run-out earthquake-induced event, but the kinematic processes are not well understood. The main objectives of this study were to numerically model the landslide progression and to reproduce the post-failure configuration. We first built a physical model of the slope based on the topography and geology of the source area from field investigations. The corrected baseline and filtered actual ground motions were then used as the volume force acting on the base block, and the kinematic process and mechanics of the throwing phenomenon were modelled using a 2-D discrete element code. We used the non-linear Barton–Bandis criterion to accurately simulate the behaviour of joints.

The size effect of the enormous landslide was also considered. The results of the simulations agreed well with those obtained from post-earthquake field investigations. A sensitivity analysis of several related parameters that may control the dynamic movements of the Donghekou landslide was discussed in detail. The results show that: the seismic force and the residual friction angle were main factors that affect the run-out of landslides.

**Keywords** Donghekou landslide · Rapid long run-out · Kinematic processes · 2-D discrete element code · The “ejection” phenomenon

---

Z.-C. Song · L.-H. Zhao (✉) · L. Li · G. Tang  
School of Civil Engineering, Central South University,  
Changsha 410075, Hunan, China  
e-mail: zlh8076@163.com

Z.-C. Song  
e-mail: songzhichen1219@163.com

G. Tang  
e-mail: tgpcsu@gmail.com

L.-H. Zhao  
Key Laboratory of Heavy-Haul Railway Engineering  
Structure, Ministry of Education, Central South  
University, Changsha 410075, Hunan, China

Y. Zhang (✉)  
Key Laboratory of Transportation Tunnel Engineering,  
Ministry of Education, Southwest Jiaotong University,  
Chengdu 610031, China  
e-mail: yingbinz516@126.com

Y. Zhang  
Department of Geotechnical Engineering, School of Civil  
Engineering, Southwest Jiaotong University,  
Chengdu 610031, China

## 1 Introduction

Earthquakes are considered to be the main triggers of numerous large-scale landslides over areas of more than one million km<sup>2</sup> (Li et al. 2012). Large-scale landslides caused by earthquakes have claimed tens of thousands of lives and caused innumerable property losses. For example, 9272 landslides were triggered by the 1999 Chi–Chi earthquake ( $M_s = 7.6$ ) in Taiwan and caused more than 10,000 deaths and economic losses of more than 10 billion US\$ (Chang et al. 2005). To analyse catastrophic earthquake-induced landslide hazards, in addition to needing detailed information about the earthquake and hypocentral region, it is critical to determine the failure mechanism of catastrophic earthquake-induced landslides.

The Wenchuan earthquake triggered thousands of mountain movements in the Longmen Mountains region, some of which caused many casualties and property losses. High-speed and long run-out landslides triggered by earthquakes are one of the most common destructive geological hazards because of their large volumes. The Donghekou landslide is a typical high-speed and long run-out landslide that was triggered by the Wenchuan earthquake (Sun et al. 2009).

After the Donghekou landslide, several field investigations were performed to map the post-landslide topography and identify the failure mechanisms (Yin 2008; Wang et al. 2009; Huang and Fan 2013). Furthermore, numerical simulations based on different field investigations have been widely used to study the movement process of the landslide (Zhang et al. 2014; Yuan et al. 2013). Nevertheless, due to the complex kinematic processes and some special phenomenon, the initial triggering process and the internal mechanism that affects the movement of large-scale landslides are still not well understood.

The complex kinematics of landslides are controlled by the morphological and geological features of the slope as well as the mechanical properties of the slope surface and the triggering process. By far, many studies have investigated the dynamic processes of landslides triggered by the Wenchuan earthquake and the research methods can be classified into several categories: (1) continuous method, such as the finite element method (McDougall and Hungr 2004; Crosta et al. 2009a, b; Chen et al. 2006; Favreau et al. 2012), boundary element (Wang et al. 2011) etc.; (2)

discontinuous method, (Zhang et al. 2011; Huang 2009; Cui et al. 2011; Bai et al. 2014; Kuo et al. 2014); (3) limit equilibrium method (Thiebes et al. 2014; Zhou and Cheng 2014; Saade et al. 2016). However, traditional continuum models neglect the contacts between rocks, which make it impossible to trace the positions of individual rocks during a landslide. In contrast, discontinuous numerical simulation methods are powerful tools for simulating failure processes of rock avalanches that are controlled by surfaces of weakness (Zhang et al. 2015; Staron 2008).

The most appropriate method in many dynamic response and collapse simulations of jointed rock slopes during earthquakes is the discrete element analysis. Two kinds of discrete element analysis are currently widely used. One is discontinuous deformation analysis (DDA), which is a new method of calculating the strains and displacements of a block system and was proved to be a very powerful tool to simulate the failure and run-out process of rock avalanche (Zhang and Yin 2013; Bakun-Mazor et al. 2012; Yagoda-Biran and Hatzor 2010). The other is the discrete element method (DEM), which is widely used for kinematic analyses of geomaterials under quasi-static or dynamic conditions (Xu et al. 2015; Wang et al. 2014a, b, c; Ma et al. 2014; Gu and Huang 2016). Both methods are derived from rock mechanics and are solved using the improved Lagrange equation. The main difference between the two is the equation of motion that is established. The former is calculated using the implicit equation, while the latter uses the explicit solution.

The DEM considers the system as being composed of discrete individuals, which have the characteristics of contact and detachment, relative movement and a relationship between the contact force and energy. It can be used to solve the macroscopic mechanical behaviour of joints and cracks, which is a limitation of DDA. The discrete element method can be coupled to other numerical methods to increase the advantages of both methods. For example, the influence of the far field stress can be considered by using the boundary element method to simulate elastic properties, the finite element method can then be used as a transition to consider plastic deformation, and the DEM can finally be used to consider the discontinuous near field deformation. The combination of methods has greatly extended the range of applications of the numerical methods.

This paper studies the process of the Donghekou landslide due to the earthquake and attempts to reproduce the post-failure configuration. Toward this, the 2-D discrete element method is used for this simulation and to identify the phenomenon.

## 2 Overview of the Donghekou Landslide

The  $M_w = 7.9$  Wenchuan earthquake occurred in Sichuan Province, China at 14:28 CST on 12 May 2008. The epicentre was located approximately 80 km west-northwest of Chengdu, and the hypocentre was at a depth of approximately 19 km (Fig. 1a). This area is one of the most significant regions of deformation in mainland China due to the large number of seismically active faults (Dai et al. 2011; Gorum et al. 2011; Jia et al. 2015; Chao et al. 2012). According to site investigations, the rupture initiated in the southern Longmen Mountains and propagated toward the northeast for approximately 300 km with both reverse and right-lateral strike-slip movements (Xu et al. 2009).

The Donghekou landslide (32.40572°N, 105.11081°E) is located in Donghekou village, Qingchuan County, approximately 250 km from Chengdu in a mountainous region at the northern termination of the Beichuan rupture zone (Fig. 1a). The landslide area is along the Longmen Mountain Fault, where the geological and topographical features are extremely complex due to the rugged topography, steep high mountains, deep valleys and complicated geologic structures (Qi et al. 2011). Figure 2 shows a view of the erosion after the occurrence of the Donghekou landslide, which had an estimated volume of approximately 24 million  $m^3$ , is at elevations of approximately 1150 to 1350 m. It travelled downhill and destroyed almost all of the houses near the erosion area, generating approximately 780 mortal casualties (Yin et al. 2009).

The primary factor of the Donghekou landslide is the collapse of the trailing edge bedrock and top cover along the bedrock during the strong earthquake. Due to the significant horizontal and vertical seismic accelerations, the sliding body was thrown along the direction of the slope (N60°E). A crack then occurred along the structural plane of the rock mass and opened. Subsequently, the sliding body collided violently with the slope, and the high potential energy was transformed into kinetic energy of the sliding body, which

led to crushing and complete disintegration of the rock into high-speed debris. The rockslide–debris was limited by the gully and the slope terrain in the main sliding direction. The main part of the slide body turned into the gully and moved towards the northeast for approximately 2.5 km to the junction between the Qingzhu and Hongshi rivers and formed a dammed lake.

## 3 Geological Setting of the Donghekou Area

The initiation region of the landslide, Daping Mountain, is 1609.6 m high and has an average slope of approximately 40°. The local mountain surfaces are as steep as 70°–80°. The elevations of both sides of the landslide zone are above 1000 m, and the trailing edge elevations are up to 1400 m with a relative height of more than 700 m compared to the river valley. The large difference in height generated significant potential energy that provided favourable conditions for eroding the high position of the sliding body.

As shown in Fig. 1b, the exposed materials along the slope are mainly dolomitic limestone and siliceous phyllite. The former, which has an orientation of 26°/041° (dip and inclination direction, respectively, see Fig. 3), was mostly concentrated in the rock collapse zone on the northwest side of the landslide, and only a few limestone outcrops were observed at the top of the slope. The latter, which has an orientation of 28°/040°, was mainly located in the main landslide zone and in the area of domino-shaped ground tension cracks.

## 4 Estimate of Rock Strength Considering the Effect of Block Size

The scale of the slope influences the rock strength, which can be reflected by the nonlinear failure criterion of the material. Traditional slope stability calculations are based on the linear Mohr–Coulomb failure criterion. However, numerous studies have shown that the strength envelopes of almost all materials are nonlinear. Although the nonlinear relationships are not obvious at low confining pressures, which have an insignificant effect on the friction angle, the nonlinear characteristics of the rocks become increasingly significant at higher confining pressures and cannot be ignored. The Donghekou

**Fig. 1** Main area of shaking due to the Wenchuan earthquake. **a** Regional structures (modified from Wang et al. 2014a, b, c) and **b** geological map of the Donghekou landslide (modified from Wang et al. 2014a, b, c)

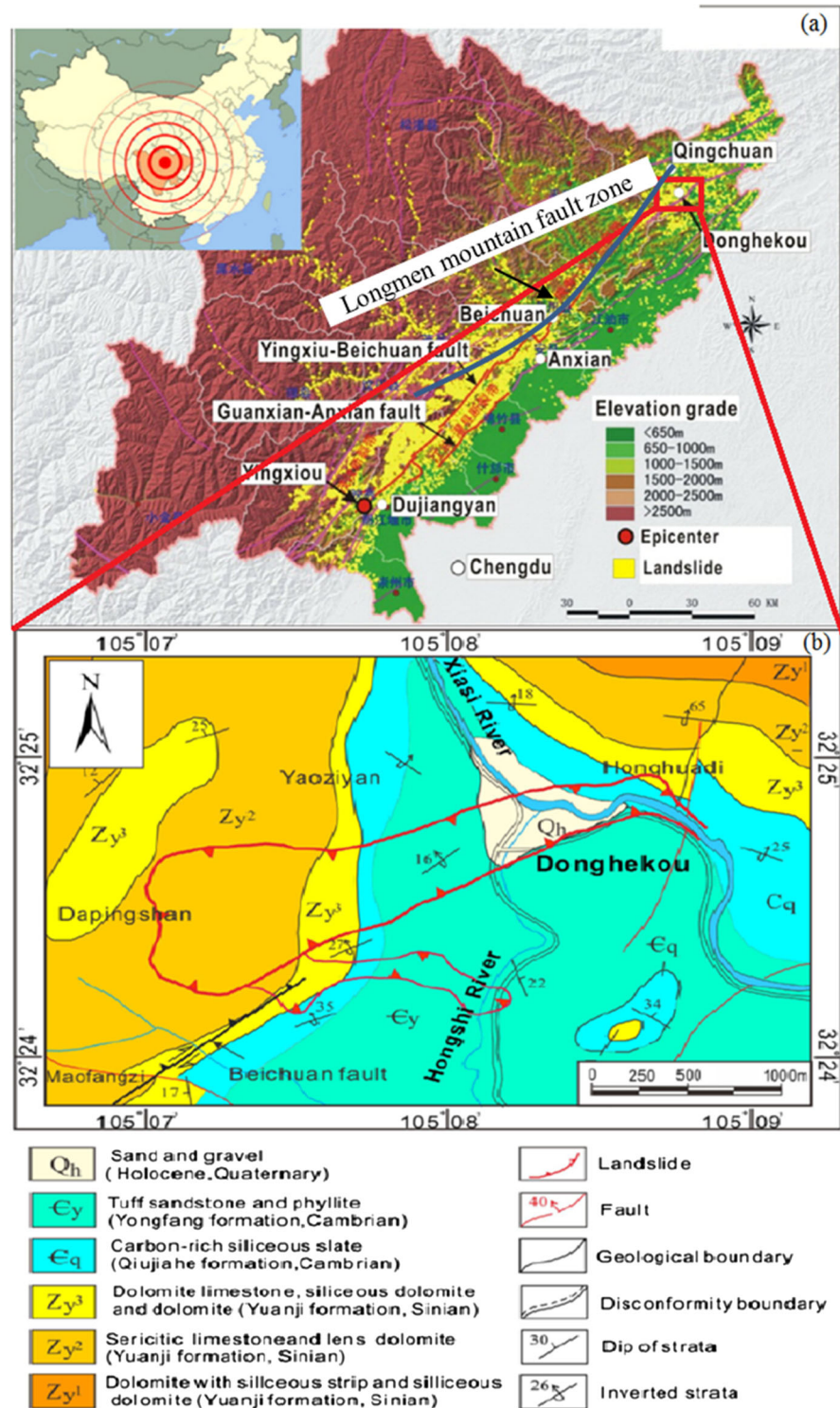




**Fig. 2** The Donghekou landslide (modified from Wang et al. 2014a, b, c). **a** The region before the earthquake. **b** Qingzhu dammed lake and **c** 2 months after the earthquake

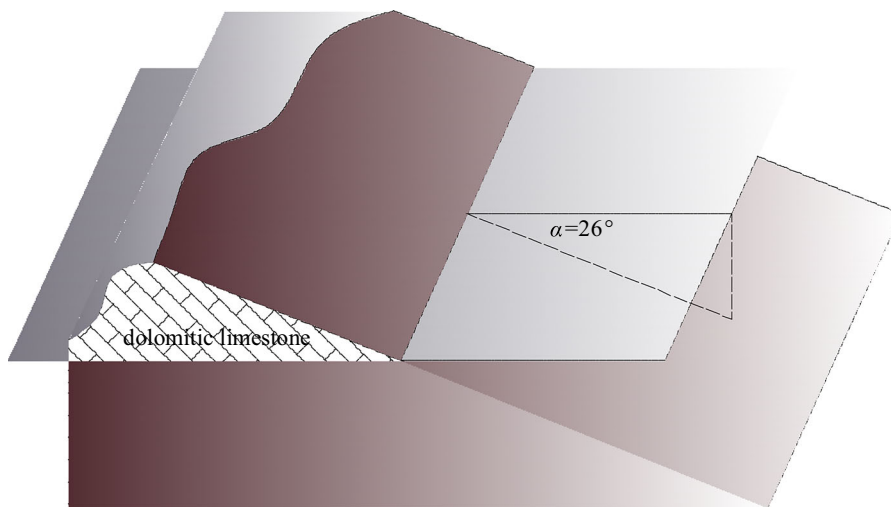


**Fig. 3** Schematic diagram of strata attitude

landslide has a volume of approximately 24 million m<sup>3</sup>, so the variation of the rock strength due to the scale of the landslide must be considered.

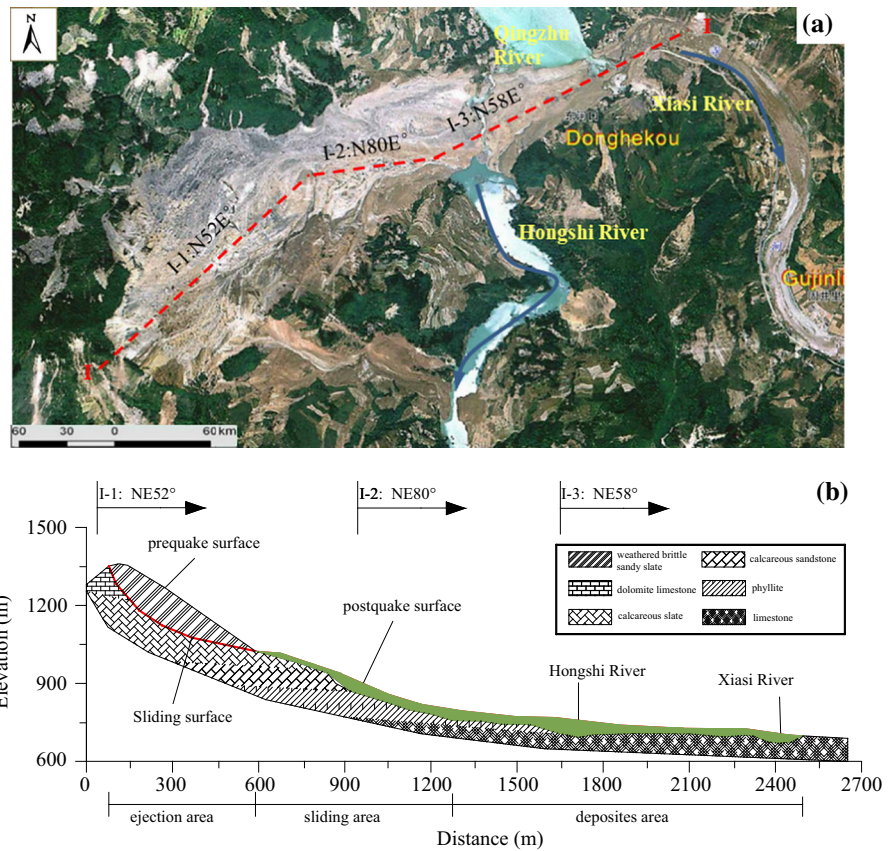
We use the nonlinear failure criterion to consider the effect of the slope size on the rock strength. In this paper, the nonlinear failure criterion is used to back-

calculate the material parameters of the rock mass. The stability of the rock mass slope is greatly influenced by the shear strength of the structural plane. Barton and Bandis proposed the nonlinear Barton–Bandis (BB) criterion based on the analysis of shear test data of a large number of structural planes.

**Table 1** BB joint parameters and intact rock parameters assumed for the Donghekou landslide simulations

Parameters	Values
Joint roughness coefficient, $JRC_0$	10
Joint compressive strength, $JCS_0$ (MPa)	80
Residual friction angle, $\varphi_r$ (°)	12
Uniaxial compressive strength, $r_c$ (MPa)	100
Unit weight of the Donghekou sliding mass, $g$ (kN/m <sup>3</sup> )	21.5
Unit weight of the landslide base, $g$ (kN/m <sup>3</sup> )	25
Deformation modulus of the Donghekou sliding mass (GPa)	12.6
Deformation modulus of the landslide base (GPa)	34.2
Poisson's ratio of the Donghekou sliding mass (m)	0.28
Poisson's ratio of the base (m)	0.1

**Fig. 4** The Donghekou landslide induced by the Wenchuan earthquake. **a** Air photo (modified from Yin et al. 2009) and **b** I–I cross-section of the landslide



The BB criterion is applicable to the shear strength failure criteria for structural planes in the range of stresses involved in the slope and is also known as the  $JRC$ – $JCS$  yield criterion (Barton and Choubey 1977):

$$\tau = \sigma_n \tan \left[ \varphi_r + JRC \log_{10} \left( \frac{JCS}{\sigma_n} \right) \right] \quad (1)$$

where  $\sigma_n$  is the effective normal stress of the joint,  $JRC$  is the joint roughness coefficient ( $0^\circ$ – $20^\circ$ ),  $JCS$  is the joint compressive strength,  $\varphi_r$  is the residual friction angle of the joint, and  $\tau$  is the peak shear strength.

The essential input parameters of the joints for the Universal Distinct Element Code (by Itasca, in Minneapolis-MN, USA) analysis with the BB model

were obtained from a field investigation of discontinuities and shear tests in the laboratory. The joint shear strength parameters *JRC* and *JCS* were estimated based on matching of roughness profiles and Schmidt hammer tests in the proximity of the slope, respectively. The empirical relationship to estimate  $\varphi_r$  from the residual tilt tests was:

$$\varphi_r = (\varphi_b - 20^\circ) + 20(r/R) \tag{2}$$

where  $\varphi_b$  is the basic friction angle estimated from experimental statistical data; *R* is the Schmidt rebound on dry unweathered sawn surfaces, and *r* is the Schmidt rebound on wet joint surfaces.

The scale correction for the in situ block size ( $L_n$ ) is derived using the following scale correction equations (Barton and Bandis 1991):

$$\begin{cases} JRC_n = JRC_0 \left(\frac{L_n}{L_0}\right)^{-0.02JRC_0} \\ JCS_n = JCS_0 \left(\frac{L_n}{L_0}\right)^{-0.03JCS_0} \end{cases} \tag{3}$$

where the subscripts (0) and (n) refer to the lab scale (0.1 m) and in situ block sizes, respectively.

The size effect also has a significant impact on the *JRC*. The longer the base length considered, the smaller the fluctuations in the structural plane will be, which leads to a decrease of the *JRC* value. As the length of the joint wall increases, the peak shear strength decreases for various *JRC–JCS* values. For this case, a *JRC*<sub>0</sub> value of 10 gives a *JRC*<sub>n</sub> value of 7.13 when corrected to full scale ( $L_n$ ). Likewise, a *JCS*<sub>0</sub> value of 100 MPa gives a *JCS*<sub>n</sub> value of 80 MPa when corrected to full scale.

The shear (*G*) and bulk (*K*) moduli of the rock mass are calculated using the following relations:

$$\begin{cases} G = \frac{E}{2(1+\nu)} \\ K = \frac{E}{3(1-2\nu)} \end{cases} \tag{4}$$

where *E* is the deformation modulus, and  $\nu$  is Poisson’s ratio. The rock mass deformation modulus is estimated from the Q-system relation (Barton et al. 1974), where the Q-values of the base and sliding part are estimated to be approximately 40 for good rock masses and 2 for poor rock masses:

$$\begin{cases} E_{\text{mean-base}} \approx 10 \times Q_{\text{base}}^{1/3} = 34.2 \text{ GPa} \\ E_{\text{mean-sliding}} \approx 10 \times Q_{\text{sliding}}^{1/3} = 12.6 \text{ GPa} \end{cases} \tag{5}$$

Table 1 shows the mechanical properties of the intact rock and the BB joint shear strength parameters (*JRC*, *JCS* and  $\varphi_r$ ) adopted for the modelling studies.

## 5 Distinct Element Modelling

### 5.1 Problem Setup and Basic Assumptions

The Donghekou landslide is a typical large-scale and high-speed long run-out landslide that was induced by the Wenchuan earthquake. Figure 4a shows an air photo of the Donghekou rockslide, and Fig. 4b shows section I–I across the landslide. The central axis of the landslide is oriented N60°E. Several assumptions were made to capture the main features of the large rock avalanche:

1. The sliding body is divided into small pieces by pre-existing joints;
2. The geometry of the slope is simplified;
3. The seismic force acts only on the bottom of the block;
4. The rock below the slip surface is regarded as a homogeneous base.

#### 5.1.1 Mesh Size

In the numerical simulation, the mesh size of the model has a significant influence on the simulation results. In general, the smaller the mesh size is, the higher the calculation accuracy will be, but an excessively small mesh size will greatly increase the computational cost. To accurately simulate the propagation of seismic waves in the rock mass and to minimize the distortion of the wave at the same time, the maximum frequency ( $f_{\text{max}}$ ) of the input wave is calculated by Eq. (6) (Kuhlemeyer and Lysmer 1973):

$$f_{\text{max}} = \frac{c}{\lambda} = \frac{c}{10\Delta l} \tag{6}$$

where  $\lambda$  is the maximum wavelength (m);  $\Delta l$  is the largest spatial element size in the direction of wave propagation (m);  $c = \min(C_p, C_s)$ , and  $C_p$  and  $C_s$  represent the P wave velocity and the S wave velocity,

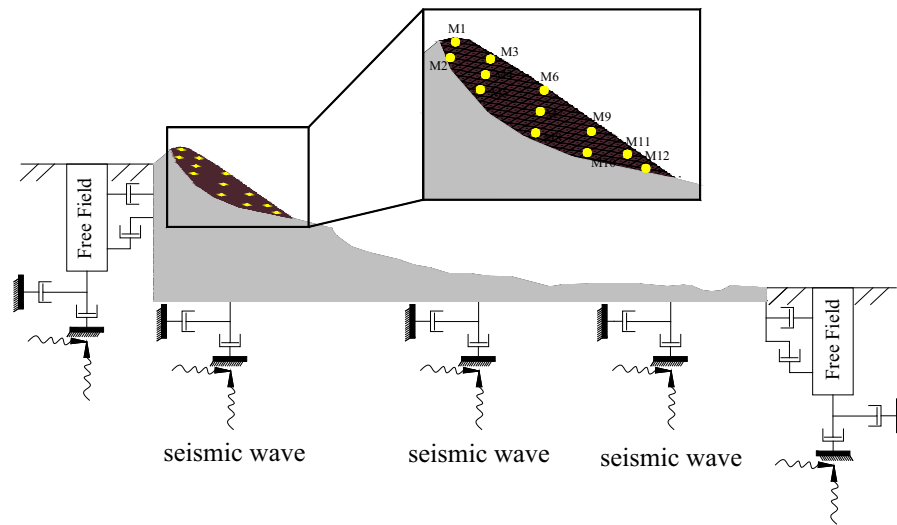


**Fig. 5** Locations of key points and boundary conditions of the landslide

respectively. The values of  $C_p$  and  $C_s$  are generally determined by field tests, since it is difficult to test directly, a feasible approach to estimate the values through Eq. (7):

$$\begin{cases} C_p = \sqrt{\frac{K + 4G/3}{\rho}} \\ C_s = \sqrt{G/\rho} \end{cases} \quad (7)$$

where  $K$ ,  $G$  and  $\rho$  are the bulk modulus (MPa), shear modulus (MPa) and density ( $\text{kg/m}^3$ ) of the rock mass, respectively.

Based on this analysis, substituting the related values into Eqs. (6) and (7) gives a maximum frequency of the input wave  $f_{\max}$  of 18 Hz, which is higher than the actual input seismic wave frequency (10 Hz) and indicates that the selected mesh size meets the accuracy requirements. In order to illustrate the velocity and displacement during sliding, some monitored blocks (marked M1–M12) have been set within the sliding body. Figure 5 shows the discrete element model configuration of the Donghekou landslide.

The selection of the model boundary conditions is an important topic in dynamic analysis. To reduce the error caused by the truncation boundary, an artificial boundary is generally used for numerical simulations. Applying tangential and normal dashpots to the boundary can absorb the wave energy; that is, the

dashpots generate normal and tangential forces to offset the stress caused by the reflection wave. Therefore, in the analysis of the dynamic seismic effect in the discrete element model, a viscous boundary is applied to the base, and free field boundaries are applied to both sides, which prevents the divergence of the reflection and the energy of the seismic waves towards the outside. However, because the force on the viscous boundary is calculated from the velocity component on the boundary, to avoid the failure of viscous boundary, the velocity wave should be transformed into a stress wave through Eq. (8) instead of applying it to the viscous boundary directly.

$$\begin{cases} \sigma_n = 2(\rho C_p)v_n \\ \sigma_s = 2(\rho C_s)v_s \end{cases} \quad (8)$$

where  $\sigma_n$  is the normal stress applied to the base (MPa),  $\sigma_s$  is the shear stress (MPa),  $v_n$  is the vertical velocity component of the vibration, and  $v_s$  is the tangential velocity component of the vibration. To compensate for the viscous boundary, the stress applied to the base of the model should be doubled.

### 5.1.2 Dynamic Loading

Based on information provided by the national strong motion network centre, the records of the Wenchuan earthquake wave at the Qingping strong motion



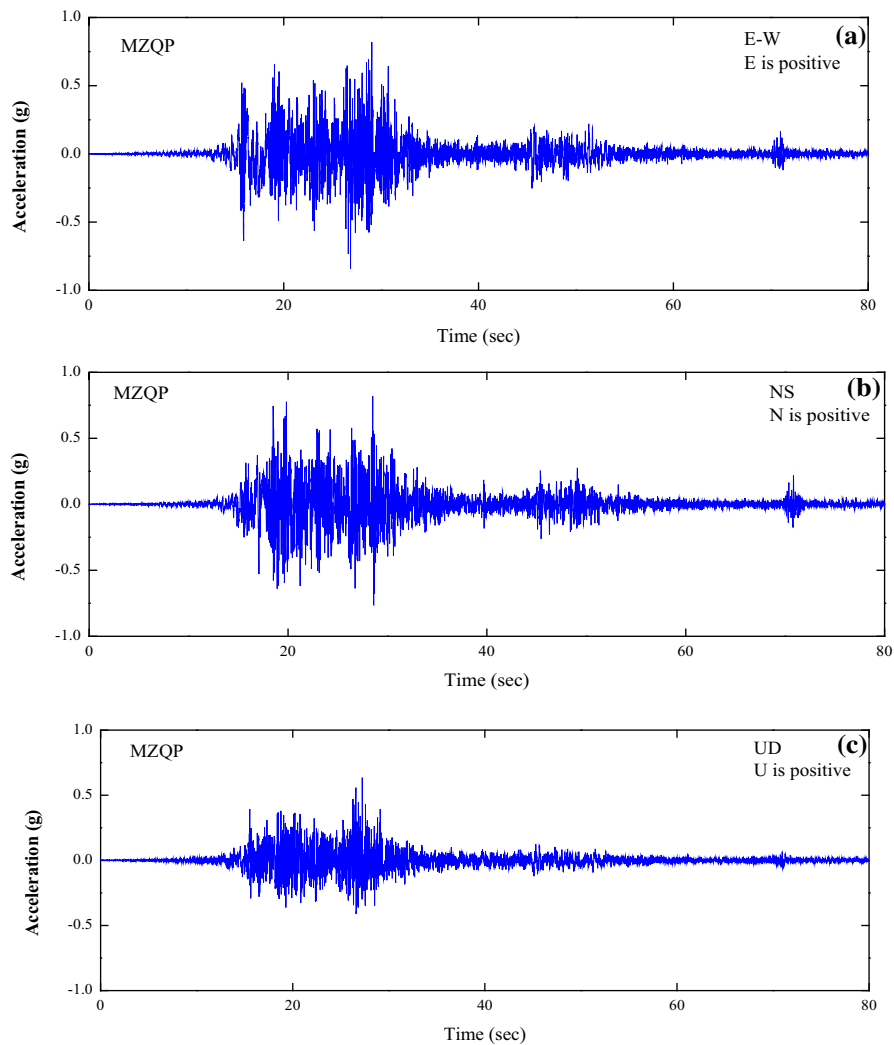


**Fig. 6** Ground acceleration records of the Wenchuan earthquake from strong motion station MZQP. **a** East–west (EW) acceleration time history curve. **b** North–south (NS) acceleration time history curve. **c** Up–down acceleration time history curve

station, which is located near the main earthquake fault zone (Yingxiu–Beichuan Fault), were used for the dynamic loading, including three directions (E–W, N–S and U–D). Figure 6 shows the three ground motion acceleration waveforms after digital processing.

The orientation of the Donghekou landslide is N60°E, so it is at an angle to the east and north directions. To facilitate the calculation, the accelerations in the two horizontal directions are projected into the slope direction (*x* direction), and algebraic

superposition is then performed. As shown in Fig. 7,  $\beta$  is the angle between the landslide direction and north,  $a_{E-W}$  and  $a_{N-S}$  are the earthquake accelerations in the east–west and north–south directions, respectively, and  $a_x$  is the horizontal earthquake acceleration in the direction of the slope, which is calculated using Eq. (9):

$$a_x = a_{E-W} \cdot \sin \beta + a_{N-S} \cdot \cos \beta \tag{9}$$

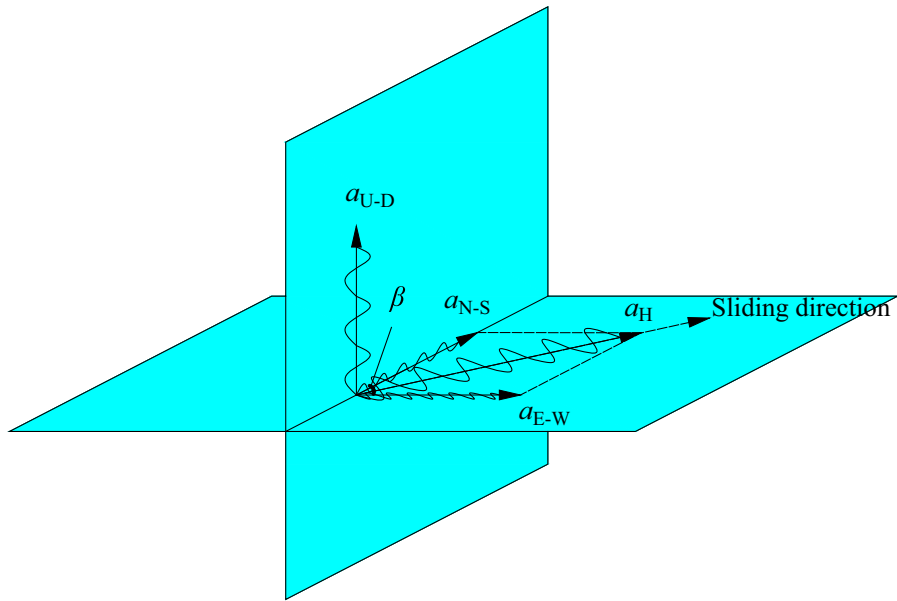


**Fig. 7** Synthesis of earthquake accelerations

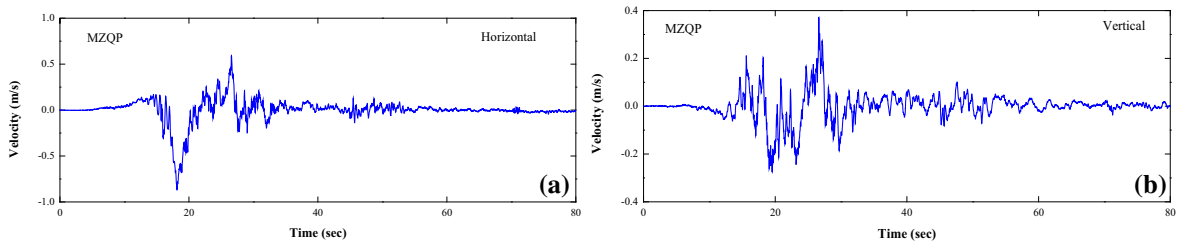


**Fig. 8** Input post-corrected and filtered **a** horizontal and **b** vertical ground velocity records

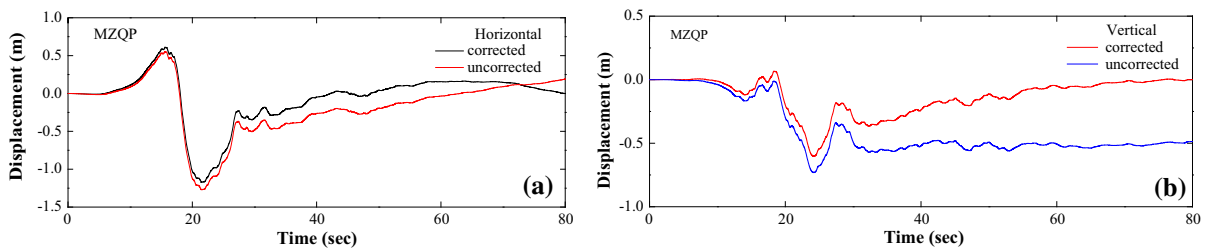


**Fig. 9** Input post-corrected **a** horizontal and **b** vertical ground displacement records

In this case,  $\beta$  is  $60^\circ$ . The dynamic wave in the  $y$  direction of the model derived from the U–D acceleration time history recorded by MZQP station.

### 5.2 Filtering and Baseline Correction

For the dynamic calculations in UDEC, higher input frequencies of the seismic wave require smaller grid cells in the model, which may affect the calculation

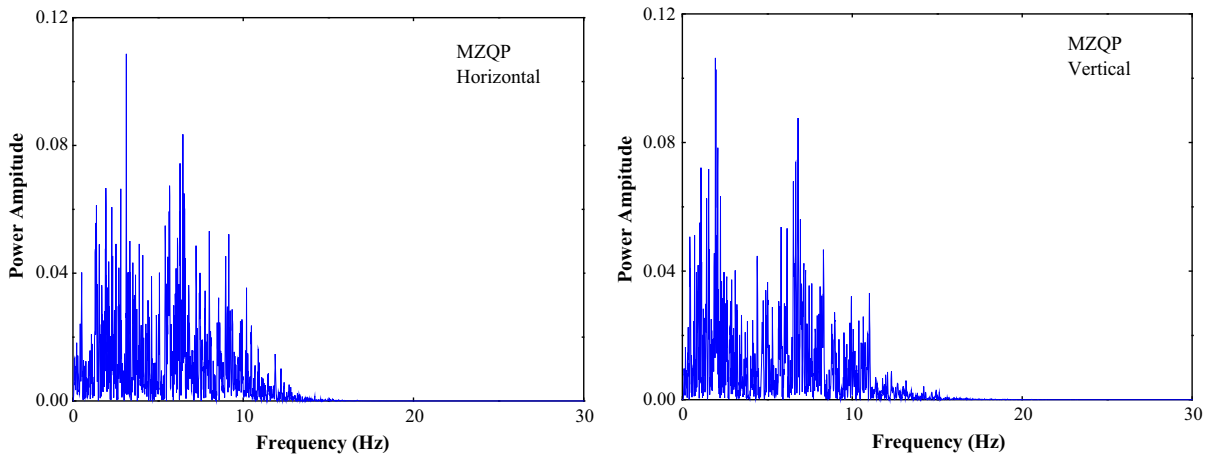


**Fig. 10** Fourier spectra of the filtered input seismic wave

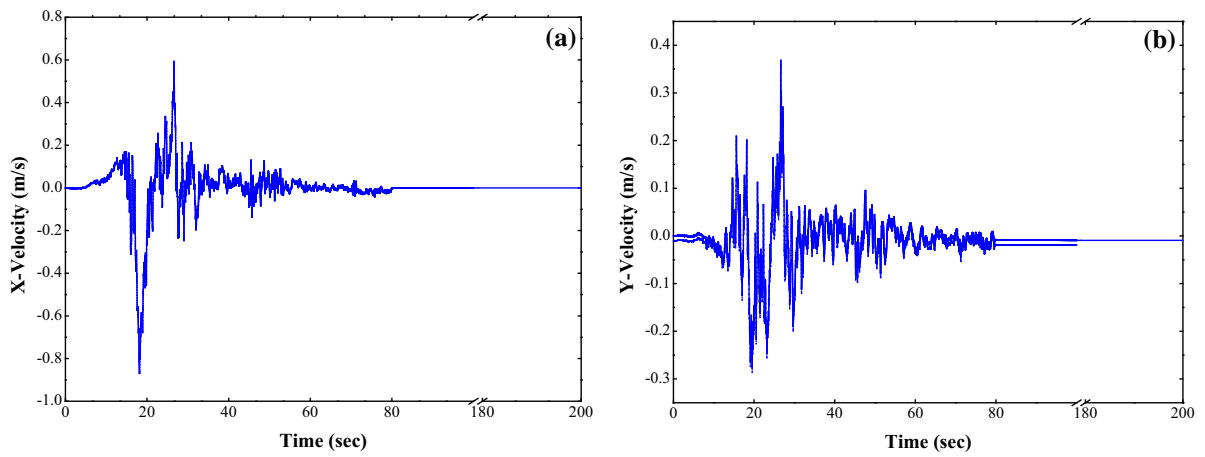


**Fig. 11** Velocity responses at the base of the model: **a** horizontal velocity response and **b** vertical velocity response

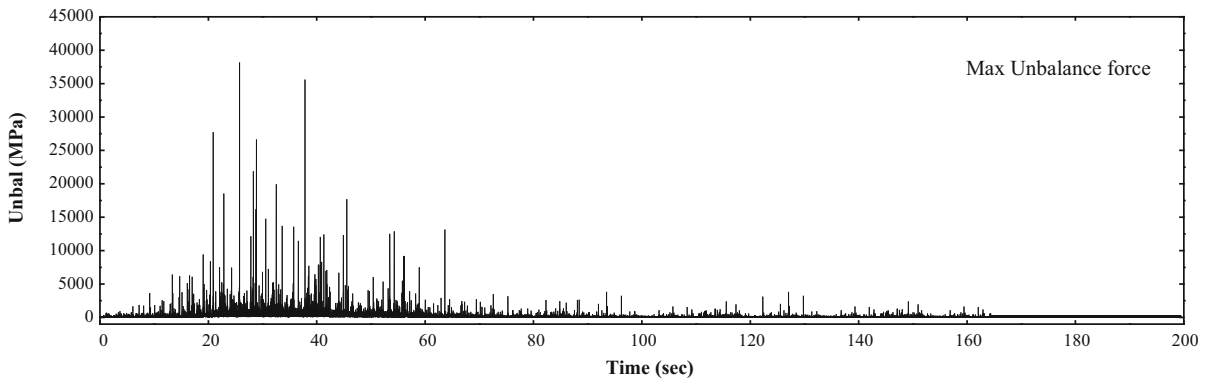


**Fig. 12** Maximum unbalanced force

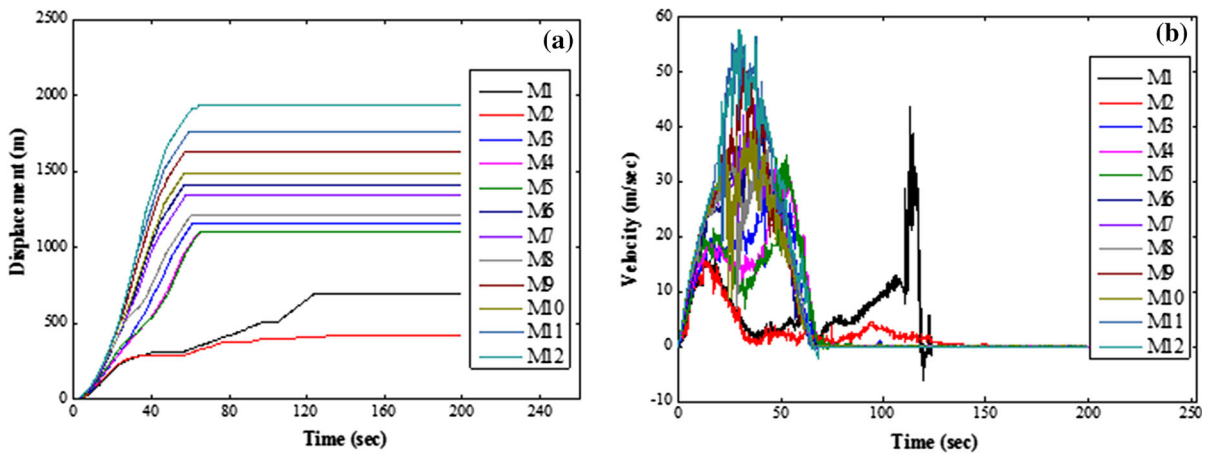


Fig. 13 Histories of key points: a displacement history and b velocity history

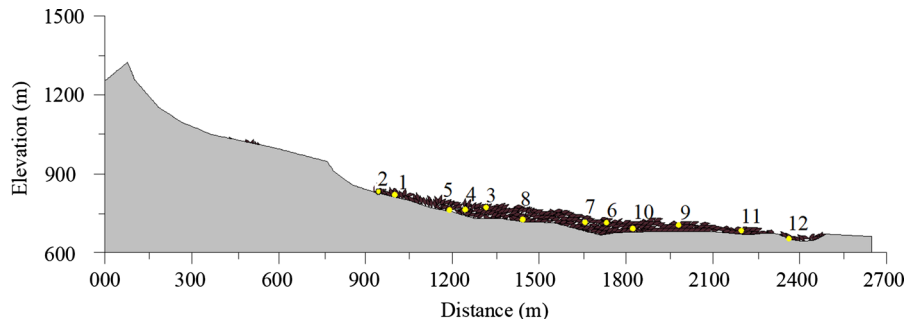


Fig. 14 Final positions of the monitored blocks

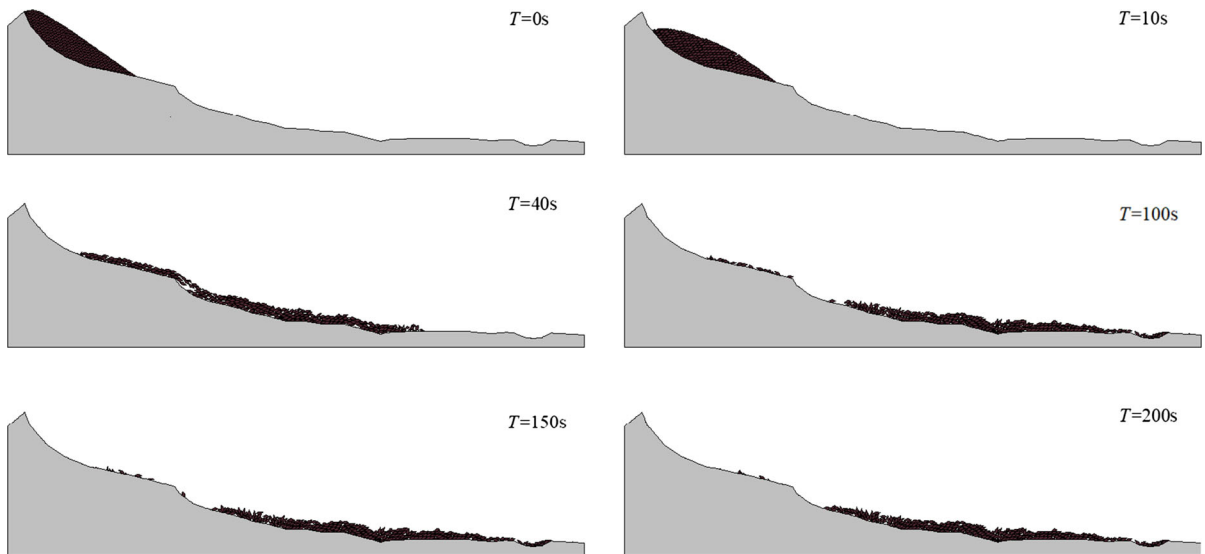
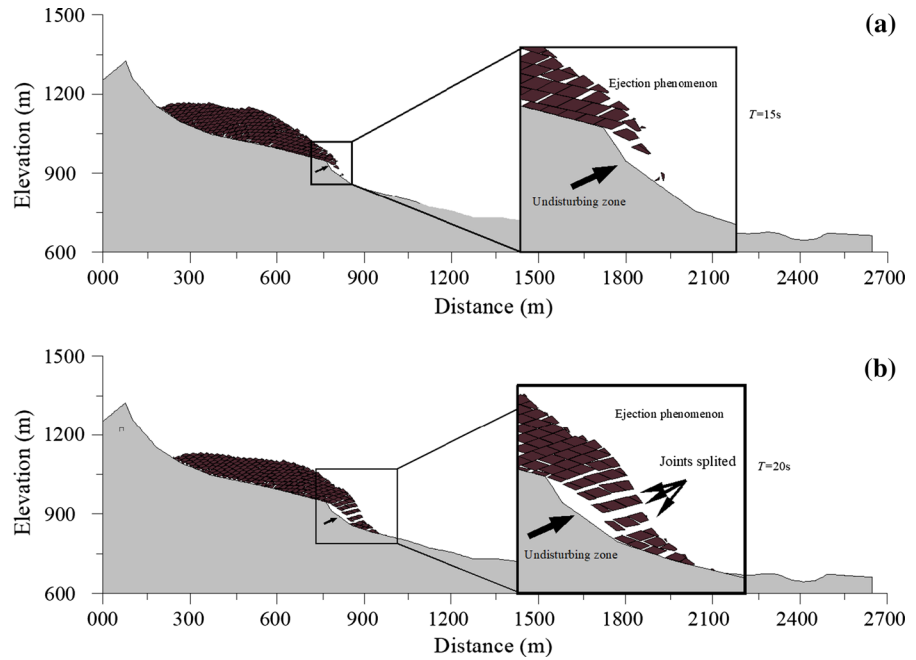


Fig. 15 UDEC simulation results of the Donghekou landslide process

**Fig. 16** Ejection phenomenon of the Donghekou landslide



**Fig. 17** The undisturbed zone remaining after the landslide

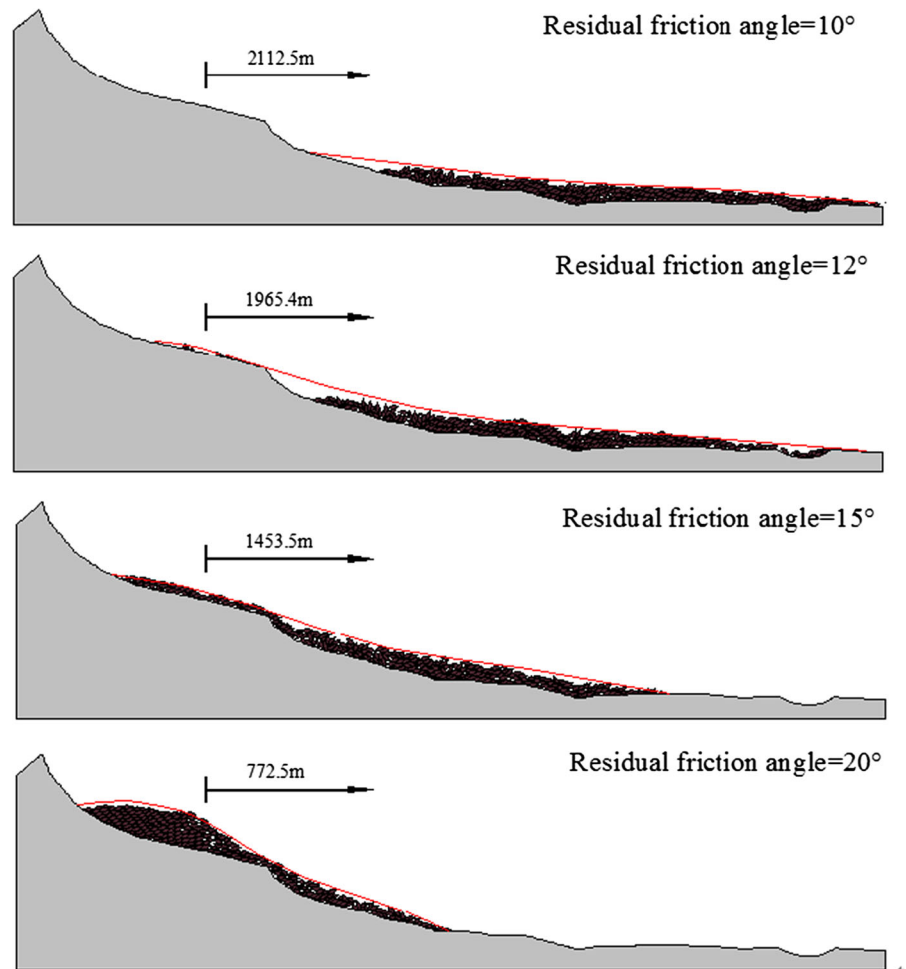
speed and result in unnecessary waste. To improve the computational efficiency, the earthquake wave must be filtered. The seismic velocity time history curves after filtering and baseline correction are shown in Figs. 8 and 9, respectively, and the Fourier spectra of the input seismic wave are shown in Fig. 10.

## 6 Results

The horizontal and vertical dynamic responses at the base of the model under the seismic loads are shown in

Fig. 11. The calculated results are consistent with the input data and do not show any distortions. Figure 12 shows that although the dynamic loading ended at  $t = 80$  s, the slope was unstable at that time, and the landslide was still moving. At  $t = 200$  s, the maximum unbalanced force was small relative to the earthquake occurrence stage, which means that the landslide had reached steady state, and the landslide process had ended. The earthquake response of the landslide is most intensive at  $t = 18$ – $40$  s, and the earthquake is the direct cause of the landslide. Figure 13 shows that the lower sliding body had a longer run-out distance and higher speed due to the collision in the rear, but it stabilized faster. The upper body had a shorter run-out distance with a lower speed and stabilized more slowly because of the gravitational potential energy. The blocks in the middle section formed a disordered depositional pattern because they depleted most of their kinetic energy due to random collisions. However, the blocks may also have different run-out distances with depth inside the sliding body. For example, M2 and M5, which are located near the landslide base, have shorter run-out distances than M1, M3, and M4 (Fig. 14). In general, in the same perpendicular, the blocks from the upper layers have longer run-out distances than those in the deeper layers. This can be explained by the lower

**Fig. 18** Effects of the residual friction angle on the landslide



pressures in the upper layers and stronger amplification effect of acceleration, which lead to greater freedom to move for the blocks near the surface of the sliding body.

The progressive failure process of the Donghekou landslide during the earthquake is shown in Fig. 15. The simulation results show that the sliding face formed at approximately 10 s, when the sliding mass began to move downslope and gouge out the sliding base. The sliding body then collided with the ground and disintegrated further, which allowed it to slide further. The debris subsequently travelled a long distance to the confluence of the Qingzhujiang River and the Hongshi River, where it formed a dammed lake. Overlaying the final step of the UDEC calculation with the topographic cross-section of the

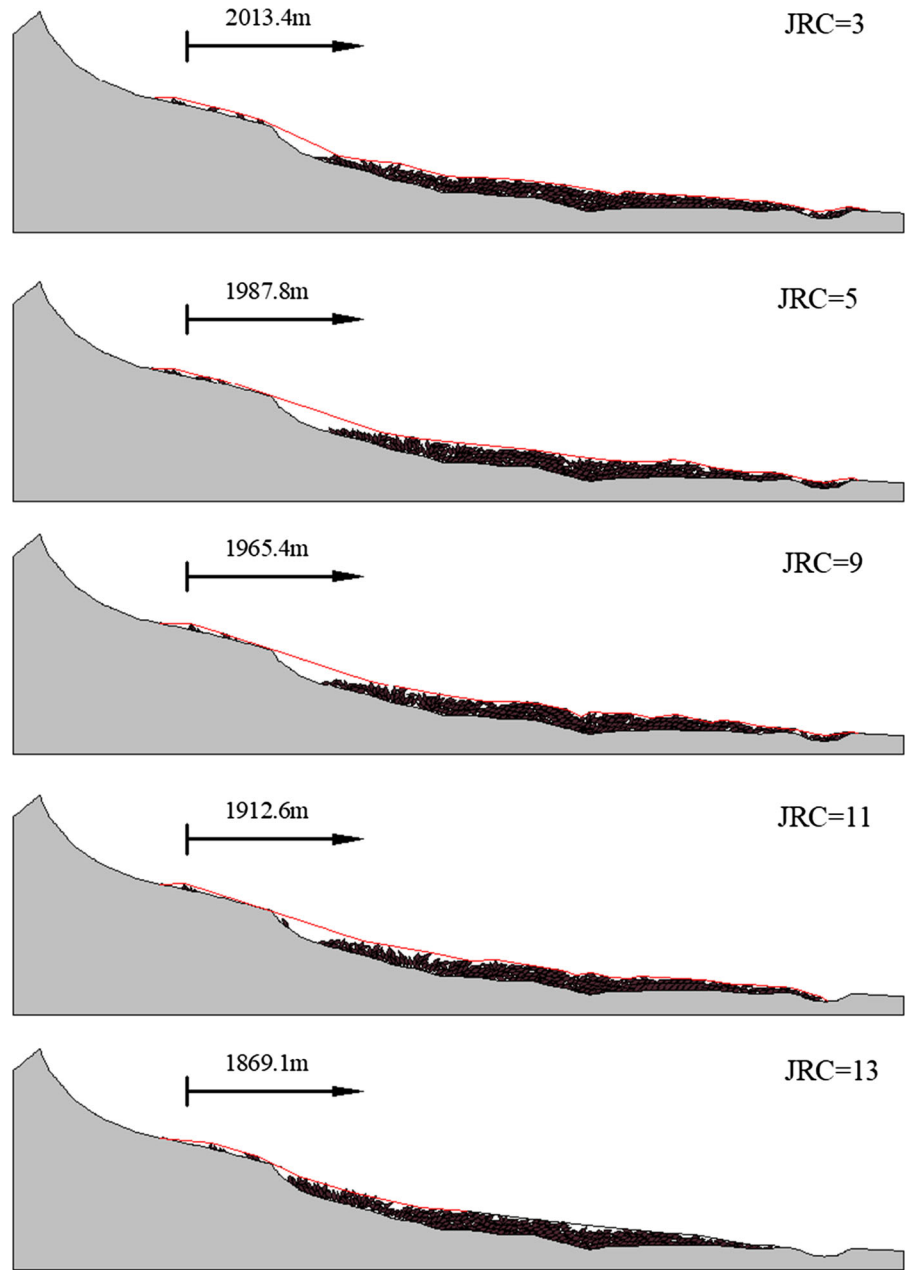
Donghekou landslide (Fig. 4) shows that the simulated depositional pattern of the Donghekou landslide under the earthquake loads is consistent with the local topography.

## 7 Discussion

### 7.1 “Ejection” Phenomenon

The simulated results show that the upper sliding body had an initial velocity during the initial stage of the landslide due to the strong earthquake action. After the sliding body separated from the upper sliding face, a free face formed, and the sliding body was then thrown out at high velocity (Fig. 16a). Following that, the

**Fig. 19** Effects of joint roughness on the landslide



sliding body was damaged as it developed additional cracks (Fig. 16b). When the projectiles hit the slope at high speed, they disintegrated into debris and then moved downslope rapidly. An undisturbed area was formed in the steep part of the slope due to the thrown debris from the coast. The field investigations confirmed the presence of an undisturbed area with clear linear motion characteristics on both sides (Fig. 17).

### 7.2 Sensitivity Analysis of Shear Strength and Joints

The Barton model test shows that when shearing occurs along a fracture surface, the shear capacity of the fracture surface is composed of two parts; one is caused by the uneven surface of the crack, and the other is caused by the friction between the contacts.

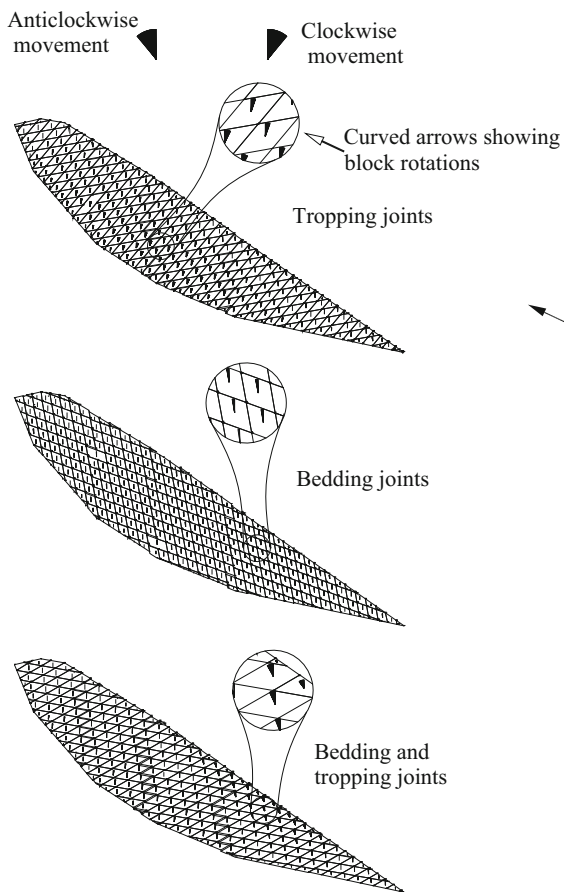


**Fig. 20** Influence of different joint types on the initial state of the earthquake-induced landslide ( $T = 0.5$  s)

The friction coefficients used in this simulation are back-calculated from empirical induction and equations based on experience, which may contain some associated uncertainties. Hence, sensitivity analyses of  $\varphi_r$  and  $JRC$  were performed to explore their impacts on the landslide process.

### 7.2.1 Role of the Joint Residual Friction Angle $\varphi_r$

While keeping the other parameters constant, four values of  $\varphi_r$  are used to study the effects of the residual friction angle on the run-out distance and final deposition. Figure 18 shows the results of the simulations, which show significant differences in the landslide process. The final topography of the deposits in the simulations indicated that the residual friction angle strongly governs the run-out distance. A comparison of the simulated results to the actual post-

landslide topography shows that the residual friction angle shown in Table 1 is most consistent with the characteristics of the actual landslide.

### 7.2.2 Role of the Joint Roughness Coefficient $JRC$

While keeping the other parameters constant, a series of  $JRC$  values are used to study the effects of the  $JRC$  on the slope run-out distance and the final deposition. Figure 19 shows the results of the simulations. Insignificant differences in the final depositional pattern are observed for the different values of the  $JRC$ , which implies that the effects of the  $JRC$  on the landslide run-out are trivial.

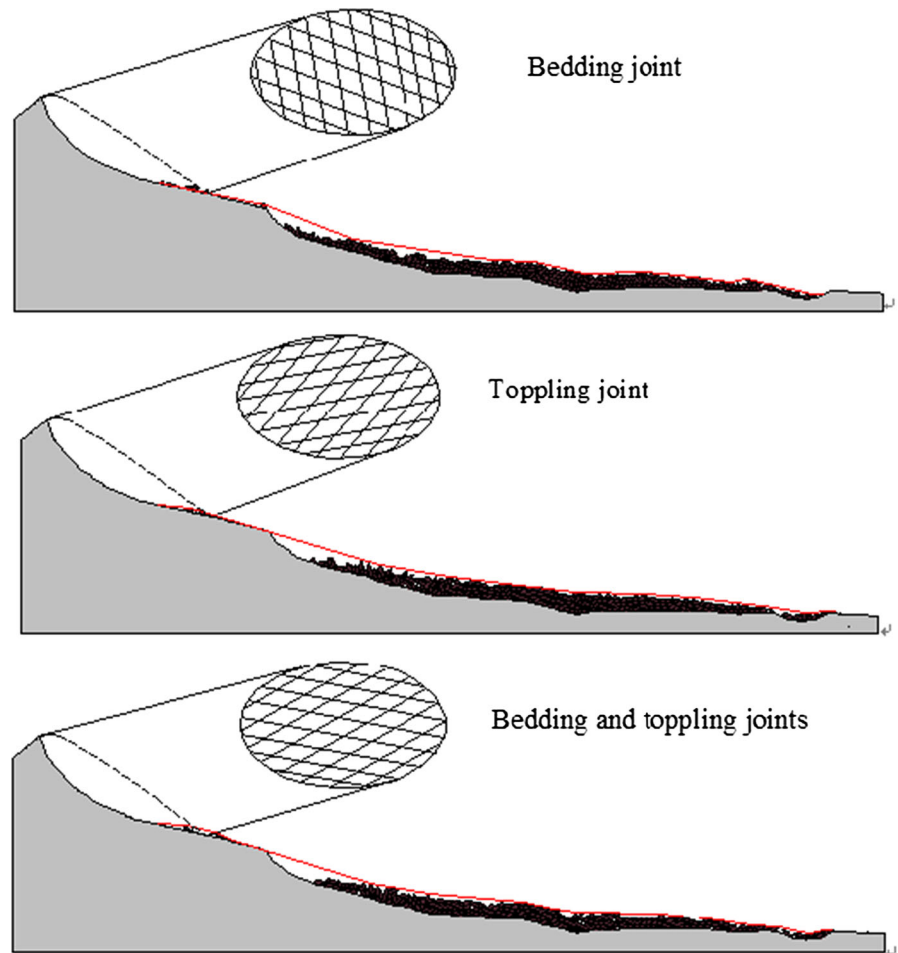
### 7.2.3 Effect of Blocks Division on the Deposition of Landslide

The pre-existing joints in the present simulation are assumed to be combined with toppling joints and bedding joints. It is necessary to reconsider the influence of other joint orientation combinations since the actual distribution of joints are unknown. Figure 20 shows the effects of three different joint types on block movement in the initial stage of earthquake triggering. The BB joint constitutive model in UDEC can simulate the phenomenon of dilation with shear. Joint dilation creates space for block rotation, while significant sliding along the discontinuities has already occurred. When considering only the toppling joints, the block has a tendency for clockwise rotation, which would result in toppling failure. Likewise, when considering only the bedding joints, the block has a tendency for anticlockwise rotation, which would result in bedding failure. However, with increasing dynamic load and detachment between the blocks, the rotation gradually changes to slippage.

Figure 21 shows the effects of the three different joint types on the final deposition of the landslide. The comparison shows that the joint type has a relatively small effect on the run-out distance of the landslide. The toppling-only type of joints results in the longest run-out distance, while the bedding-only type of joints leads to the shortest run-out. The joint type adopted in this paper accurately reflected the shape of landslide after the earthquake.



**Fig. 21** Effect of block cutting on the deposition of landslide



## 8 Conclusions

This paper mainly focuses the run-out of earthquake-induced landslides for the purpose of better understanding of post-failure behaviours of the slide. Despite several uncertainties, the simulation results are able to reproduce the entire landslide process, and the post-failure configuration resembled the geometry that was observed in the field. In addition, the simulated results showed that the large local seismic acceleration and a free face under the sliding body are responsible for the “ejection” phenomenon of the landslide. The parameter analysis showed that the residual friction angle has a significant influence on the run-out distance of the landslide and that the joint roughness coefficient has a minor influence. Although the types of joints that divided the blocks have an insignificant influence on the sliding distance of the

landslide, they affect the initial state of the landslide. How to accurately restore the distribution of joints in the slope model is still a question that is worth probing into further.

This case study demonstrates that numerical modelling utilizing information from observations and measurements (e.g., geomorphology, tectonic geology, mechanical property of materials) can be used to generate a reasonable post-failure configuration, which is important for designing remedial measures. Two-dimensional modelling can accurately explain the kinematic processes of the Donghekou landslide. However, it is unable to account for the constraints in the direction perpendicular to transport. Thus, three-dimensional modelling should be undertaken in the future to provide more accurate simulations of the debris movements and its accumulation, which require more information from a priori field measurements.

**Acknowledgements** This study was financially supported by the National Natural Science Foundation of China (Nos. 51208522, 51308551, 51478477, 51408511), Guizhou Provincial Department of Transportation Foundation (No. 2012122033) and the Fundamental Research Funds for the Central Universities of Central South University (No. 2016zzts413). All financial supports are greatly appreciated.

## References

- Bai SB, Wang J, Thiebes B et al (2014) Susceptibility assessments of the Wenchuan earthquake-triggered landslides in Longnan using logistic regression. *Environ Earth Sci* 71(2):731–743
- Bakun-Mazor D, Hatzor YH, Glaser SD (2012) Dynamic sliding of tetrahedral wedge: the role of interface friction. *Int J Numer Anal Met* 36(3):327–343
- Barton N, Bandis S (1991) Review of predictive capabilities of JRC–JCS model in engineering practice, vol 182. Publikasjon-Norges Geotekniske Institutt, Oslo, pp 1–8
- Barton N, Choubey V (1977) The shear strength of rock joints in theory and practice. *Rock Mech Rock Eng* 10(1–2):1–54
- Barton N, Lien R, Lunde J (1974) Engineering classification of rock masses for the design of tunnel support. *Rock Mech Rock Eng* 6(4):189–236
- Chang KJ, Taboada A, Lin ML et al (2005) Analysis of landsliding by earthquake shaking using a block-on-slope thermo-mechanical model: example of Jiufengershan landslide, central Taiwan. *Eng Geol* 80(s1–2):151–163
- Chao Q, Aiguo X, Yueping Y et al (2012) Numerical simulation of dynamic behavior of donghekou rockslide-debris avalanche. *J Eng Geol* 20(3):334–339
- Chen H, Crosta GB, Lee CF (2006) Erosional effects on runout of fast landslides, debris flows and avalanches: a numerical investigation. *Géotechnique* 56(5):305–322
- Crosta GB, Imposimato S, Roddeman D (2009a) Numerical modelling of entrainment/deposition in rock and debris-avalanches. *Eng Geol* 109(1–2):135–145
- Crosta GB, Imposimato S, Roddeman D (2009b) Numerical modeling of 2-d granular step collapse on erodible and nonerodible surface. *J Geophys Res* 114(F3):120–131
- Cui P, Chen XQ, Zhu YY et al (2011) The Wenchuan earthquake (May 12, 2008), Sichuan Province, China, and resulting geohazards. *Nat Hazards* 56(1):19–36
- Dai FC, Tu XB, Xu C et al (2011) Rock avalanches triggered by oblique-thrusting during the 12 May 2008 Ms 8.0 Wenchuan earthquake, China. *Geomorphology* 132(3–4):300–318
- Favreau P, Mangeney A, Lucas A, Crosta G, Bouchut F (2012) Numerical modeling of landquakes. *Geophys Res Lett* 37(15):L15305
- Gorum T, Fan X, Westen CJV et al (2011) Distribution pattern of earthquake-induced landslides triggered by the 12 May 2008 Wenchuan earthquake. *Geomorphology* 133(3–4):152–167
- Gu D, Huang D (2016) A complex rock topple-rock slide failure of an anaclinal rock slope in the Wu Gorge, Yangtze River, China. *Eng Geol* 208:165–180
- Huang R (2009) Mechanism and geomechanical modes of landslide hazards triggered by Wenchuan 8.0 earthquake (in chinese). *Chin J Rock Mech Eng* 28(6):1239–1249
- Huang R, Fan X (2013) The landslide story. *Nat Geosci* 6(5):325–326
- Jia J, Song N, Xu Z, He Z, Bai Y (2015) Structural damage distribution induced by Wenchuan earthquake on 12th may, 2008. *Earthq Struct* 9(1):93–109
- Kuhlemeyer RL, Lysmer J (1973) Finite element method accuracy for wave propagation problems. *J Soil Mech Found Div* 99(5):421–427
- Kuo LW, Li H, Smith SAF et al (2014) Gouge graphitization and dynamic fault weakening during the 2008 Mw 7.9 Wenchuan earthquake. *Geology* 42(1):47–50
- Li X, He S, Luo Y et al (2012) Simulation of the sliding process of Donghekou landslide triggered by the Wenchuan earthquake using a distinct element method. *J Environ Earth Sci* 65(4):1049–1054
- Ma G, Chang XL, Zhou W et al (2014) Mechanical response of rockfills in a simulated true triaxial test: a combined FDEM study. *Geomech Eng* 7(3):317–333
- Mcdougall S, Hungr O (2004) A model for the analysis of rapid landslide motion across three-dimensional terrain. *Can Geotech J* 41(41):1084–1097
- Qi S, Xu Q, Lan H, Zhang B, Liu J (2011) Spatial distribution analysis of landslides triggered by 2008.5.12 Wenchuan Earthquake, China. *Eng Geol* 116:95–108
- Saade A, Abou-Jaoude G, Wartman J (2016) Regional-scale coseismic landslide assessment using limit equilibrium analysis. *Eng Geol* 204:53–64
- Staron L (2008) Mobility of long-runout rock flows: a discrete numerical investigation. *Geophys J Int* 172(1):455–463
- Sun P, Zhang YS, Yin YP et al (2009) Discussion on long runout sliding mechanism of Donghekou landslide–debris flow. *J Eng Geol* 17(6):737–744
- Thiebes B, Bell R, Glade T et al (2014) Integration of a limit-equilibrium model into a landslide early warning system. *Landslides* 11(5):859–875
- Wang YS, Xu HB, Luo YH et al (2009) Study of formation conditions and toss motion program of high landslides induced by earthquake. *Chin J Rock Mech Eng* 28(11):2360–2369
- Wang Q, Qiao X, Lan Q et al (2011) Rupture of deep faults in the 2008 Wenchuan earthquake and uplift of the Longmen Shan. *Nat Geosci* 4(9):634–640
- Wang F, Sun P, Highland L et al (2014a) Key factors influencing the mechanism of rapid and long runout landslides triggered by the 2008 Wenchuan earthquake, China. *Geoenviron Disasters* 1(1):1–16
- Wang G, Huang R, Lourenço SDN et al (2014b) A large landslide triggered by the 2008 Wenchuan (M8.0) earthquake in Donghekou area: phenomena and mechanisms. *Eng Geol* 182:148–157
- Wang Z, Ruiken A, Jacobs F et al (2014c) A new suggestion for determining 2D porosities in DEM studies. *Geomech Eng* 7(6):665–678
- Xu X, Wen X, Yu G et al (2009) Coseismic reverse- and oblique-slip surface faulting generated by the 2008 Mw 7.9 Wenchuan earthquake, Chin. *Geology* 37(6):515–518

- Xu WJ, Li CQ, Zhang HY (2015) DEM analyses of the mechanical behavior of soil and soil-rock mixture via the 3D direct shear test. *Geomech Eng* 9(6):815–827
- Yagoda-Biran G, Hatzor YH (2010) Constraining paleo PGA values by numerical analysis of overturned columns. *Earthq Eng Struct D* 39(4):463–472
- Yin Y (2008) Researches on the geohazards triggered by Wenchuan earthquake, Sichuan. *J Eng Geol* 16(4):7–12
- Yin Y, Wang F, Sun P (2009) Landslide hazards triggered by the 2008 Wenchuan earthquake, Sichuan, China. *Landslides* 6(2):139–152
- Yuan RM, Tang CL, Hu JC et al (2013) Mechanism of the Donghekou landslide triggered by the 2008 Wenchuan earthquake revealed by discrete element modelling. *Nat Hazard Earth Syst* 1(6):1195–1205
- Zhang M, Yin Y (2013) Dynamics, mobility-controlling factors and transport mechanisms of rapid long-runout rock avalanches in China. *Eng Geol* 167(12):37–58
- Zhang LM, Xu Y, Huang RQ et al (2011) Particle flow and segregation in a giant landslide event triggered by the 2008 Wenchuan earthquake, Sichuan, China. *Nat Hazards Earth Syst* 11(4):1153–1162
- Zhang Y, Wang J, Xu Q et al (2014) DDA validation of the mobility of earthquake-induced landslides. *Eng Geol* 194:38–51
- Zhang Z, Wang T, Wu S et al (2015) Rock toppling failure mode influenced by local response to earthquakes. *Bull Eng Geol Environ* 75(4):1–15
- Zhou XP, Cheng H (2014) Stability analysis of three-dimensional seismic landslides using the rigorous limit equilibrium method. *Eng Geol* 174(8):87–102